Available online at www.sciencedirect.com

SciVerse ScienceDirect

Ceramics International 39 (2013) 129–141

CERAMICS INTERNATIONAL

www.elsevier.com/locate/ceramint

Facile hydrothermal synthesis of vanadium oxides nanobelts by ethanol reduction of peroxovanadium complexes

Yifu Zhang[a], Chongxue Chen[a], Weibing Wu[a], Fei Niu[a], Xinghai Liu[b], Yalan Zhong[a], Yuliang Cao[a,*], Xin Liu[c], Chi Huang[a,d,*]

[a]College of Chemistry and Molecular Sciences, Wuhan University, Wuhan 430072, PR China
[b]School of Printing and Packaging, Wuhan University, Wuhan 430072, PR China
[c]National Laboratory for Optoelectronics, Huazhong University of Science and Technology, Wuhan 430074, PR China
[d]Engineering Research Center of Organosilicon Compound and Material, Ministry of Education of China, Wuhan University, Wuhan 430072, PR China

Received 24 March 2012; received in revised form 31 May 2012; accepted 1 June 2012
Available online 15 June 2012

Abstract

$V_3O_7 \cdot H_2O$ and VO_2(B) nanobelts were successfully synthesized by a one-pot hydrothermal approach using peroxovanadium (V) complexes, ethanol and water as the starting materials. Some parameters, such as the ratio of ethanol/water, the reaction temperature and the reaction time, were briefly discussed to reveal the formation of vanadium oxides nanobelts. It was found that the ethanol was oxidized to aldehyde confirmed by the silver mirror reaction and gas chromatography. $V_3O_7 \cdot H_2O$ and VO_2(B) nanobelts could be selectively synthesized by controlling the quantity of ethanol. The possible formation mechanism of the synthesis of vanadium oxides nanobelts was proposed. The electrochemical properties of $V_3O_7 \cdot H_2O$ and VO_2(B) nanobelts were studied, and they exhibited a high initial discharge capacity of 350 mAh/g and 190 mAh/g, respectively. VO_2(M) nanobelts were prepared by the irreversible transformation of VO_2(B) nanobelts at 700 °C for 2 h under the inert atmosphere. The phase transition properties of VO_2(M) nanobelts were investigated by DSC and variable-temperature IR, which revealed that the as-obtained VO_2(M) nanobelts could be applied to the optical switching devices.

Keywords: C. Electrical properties; C. Optical properties; D. Transition metal oxides; Vanadium oxides

1. Introduction

In the past decades, nano-structured materials have been at the forefront of applied research because of their unique physical and chemical properties, which are different from their bulk materials [1–5]. One of the most dynamic research areas is the synthesis of one-dimensional (1D) nanostructures, such as nanobelts, nanowires, nanotubes, nanorods, etc. Nanobelts, as a class of 1D nanostructures with a rectangular cross section, have been the subject of intensive research due to their novel chemical and physical properties, which make them have a wide range of potential applications in fabricating nanoscale optical, electronic, optoelectronic, electrochemical, and electromechanical devices [4–9]. Moreover, hydrothermal synthesis is an effective method to fabricate 1D nanomaterials not only because of its critical temperature and pressure, but also the low cost, large scale, and wide suitability for various materials [10,11].

Vanadium oxides and their derived compounds have attracted increasing attention in recent years [12–22], because of their extensive applications in catalysts, cathode materials for reversible lithium-ion batteries, gas sensors, electrochemical and optical devices, intelligent thermochromic windows, etc. Among them, vanadium oxide hydrate $V_3O_7 \cdot H_2O$ has stimulated great interest because it can be used as the cathode materials in lithium-ion batteries [20,23,24]. Therefore, a variety of methods, such as template method [25], surfactant-assisted approach [26],

*Corresponding authors. Tel.: +86 19871 022 888; fax: +86 027 68754067.
E-mail addresses: ylcao@whu.edu.cn (Y. Cao), chihuang@whu.edu.cn (C. Huang).

0272-8842/$36.00
http://dx.doi.org/10.1016/j.ceramint.2012.06.001

and hydrothermal/solvothermal synthesis [20,23,24,27,28], have been developed to prepare $V_3O_7 \cdot H_2O$ nanostructures. However, most of these synthetic methods of fabricating $V_3O_7 \cdot H_2O$ nanostructures are either based on templates, surfactants and using some reagents which are not environmentally friendly or through a complex and lengthy route. Moreover, the preparation of $V_3O_7 \cdot H_2O$ 1D nanomaterials still remains a great challenge for materials scientists. To the best of our knowledge, the simply direct hydrothermal synthesis of $V_3O_7 \cdot H_2O$ nanobelts using peroxovanadium (V) complex compound has been rarely reported before. As the family of vanadium oxides, vanadium dioxide VO_2(B) has received much attention in the past decades, because VO_2(B) is usually as the precursor to be transformed to VO_2(R/M) [29] and also as the promising cathode materials in lithium-ion batteries [14,30–33]. Thus, a lot of techniques of preparing VO_2(B) with different morphologies have been reported [31–36]. However, the synthesis of VO_2(B) nanobelts using peroxovanadium (V) complex compound has not been reported. Moreover, as far as we know, few literatures focused on the synthesis of $V_3O_7 \cdot H_2O$ and VO_2(B) nanobelts in a single system by a facile one-pot hydrothermal method have been reported.

In this paper, we reported a low-cost and simple approach for the preparation of $V_3O_7 \cdot H_2O$ and VO_2(B) nanobelts by a facile one-pot hydrothermal method using peroxovanadium (V) complexes and ethanol as the reductant. Some parameters, such as the ratio of ethanol/water, the reaction temperature and the reaction time, were briefly discussed to reveal the formation of vanadium oxides nanobelts. The possible formation mechanism of the synthesis of vanadium oxides nanobelts was proposed. The electrochemical properties of $V_3O_7 \cdot H_2O$ and VO_2(B) nanobelts were studied, and they exhibited a high initial discharge capacity of 350 mAh/g and 190 mAh/g, respectively. Furthermore, VO_2(M) nanobelts were prepared by the irreversible transformation of VO_2(B) nanobelts at 700 °C for 2 h under the inert atmosphere. The phase transition properties of VO_2(M) nanobelts were investigated by DSC and variable-temperature IR, which revealed that the as-obtained VO_2(M) nanobelts could be applied to the optical switching devices.

2. Experimental section

2.1. Materials

Vanadium pentoxide (V_2O_5), ethanol, and hydrogen peroxide (H_2O_2, 30 wt %) with analytical grade were purchased from Sinopharm Chemical Reagent Co., Ltd. and used without any further purification.

2.2. Synthesis of $V_3O_7 \cdot H_2O$ and VO_2(B) nanobelts

In a typical synthesis route of $V_3O_7 \cdot H_2O$ nanobelts, 5 mmol (0.91 g) of bulk V_2O_5 was dispersed in 22.9 mL of redistilled water with magnetic stirring. Then, 6.80 g of 10 wt% H_2O_2 was added into the solution and 0.1 mL of absolute ethanol was injected into above system. The solution was still stirred for 1 h at room temperature to get good homogeneity. After mixing, the mixture was transferred into a 40 mL Teflon Lined stainless steel autoclave, then sealed and maintained at 180 °C for 12 h. When the reaction was finished, the blue–green precipitates were filtered off, washed with distilled water and anhydrous alcohol several times, respectively, and dried in vacuum at 75 °C for future characterization and application. For the synthesis of VO_2(B) nanobelts, 21 mL of redistilled water and 2 mL of absolute ethanol were used and the other procedures were similar with the synthesis of $V_3O_7 \cdot H_2O$ nanobelts.

2.3. Synthesis of VO_2(M) nanobelts

To synthesize VO_2(M) nanobelts, the above VO_2(B) nanobelts was heated in a tube furnace with 5 °C/min heating rate under a flow of Ar (99.999%) gas at 700 °C for 2 h, and cooled to room temperature in the Ar flow to prevent oxidation of VO_2(M).

2.4. Characterization

X-ray powder diffraction (XRD) measurements were carried out on a D8 X-ray diffractometer equipment with Cu $K\alpha$ radiation, $\lambda = 1.54060$ Å. X-ray photoelectron spectra (XPS) was obtained on a VGESCALAB MK II X-ray photoelectron spectrometer with an exciting source of Mg Kα (1253.6 eV). The morphology of the products was observed by scanning electron microscopy (SEM, Quanta 200) and transmission electron microscopy (TEM, JEM-100CXII). The samples used for characterization were dispersed in absolute ethanol and were ultrasonicated before TEM test. Fourier transform infrared spectra (FT-IR) of the solid samples were measured using KBr pellet technique (About 1 wt% of the samples and 99 wt% of KBr were mixed homogeneously, and then the mixture was pressed to a pellet) and recorded on a Nicolet 60-SXB spectrometer from 4000 to 400 cm^{-1} with a resolution of 4 cm^{-1}. Thermo-Gravimetric Analysis and Differential Thermal Analysis (TG/DTA) measurements were performed on SETSYS-1750 (AETARAM Instruments). About 10 mg of the as-obtained samples was heated in an Al_2O_3 crucible in nitrogen atmosphere from ambient temperature to 800 °C at a constant rise of temperature (10 °C/min). The phase transition temperature of VO_2(M) was measured by differential scanning calorimetry (DSC, DSC822^e, METTLER TOLEDO) at a heating rate of 5 °C/min with a liquid nitrogen cooling system. Optical properties of VO_2(M) were tested by variable-temperature infrared spectra (variable-temperature IR, NICOLET 5700) with an adapted heating controlled cell. Variable-temperature IR spectra of the solid samples were measured using KBr pellet technique from 4000 to 400 cm^{-1} with a

resolution of 4 cm^{-1}. About 1 wt% of the samples and 99 wt% of KBr were mixed homogeneously, and then the mixture was pressed to a pellet.

2.5. Electrochemical tests

The electrochemical properties of the as-obtained $V_3O_7 \cdot H_2O$ and VO_2(B) nanobelts were tested in assembling experiment cells with metallic lithium as the negative electrode. The working electrode was made by dispersing with 85 wt % active materials ($V_3O_7 \cdot H_2O$ or VO_2(B) nanobelts), 10 wt % acetylene black carbon powder, and 5 wt % polyvinylidene fluoride (PVDF) binder in *N*-methyl-2-pyrrolidone (NMP) solvent to form a homogeneous slurry. The slurry was then spread and pressed on Al foil. The coated electrodes were dried in vacuum at 125 °C for 18 h. The electrolyte was 1 mol L^{-1} $LiPF_6$ in a mixture of ethylene carbonate (EC) and diethyl carbonate (DEC) (EC/DEC = 1/1, v/v). The cells were assembled in a glove box under an argon atmosphere. Charge–discharge tests were carried out in a voltage range 4.0–1.5 V and current densities of 30, 50, 100 and 200 mA/g.

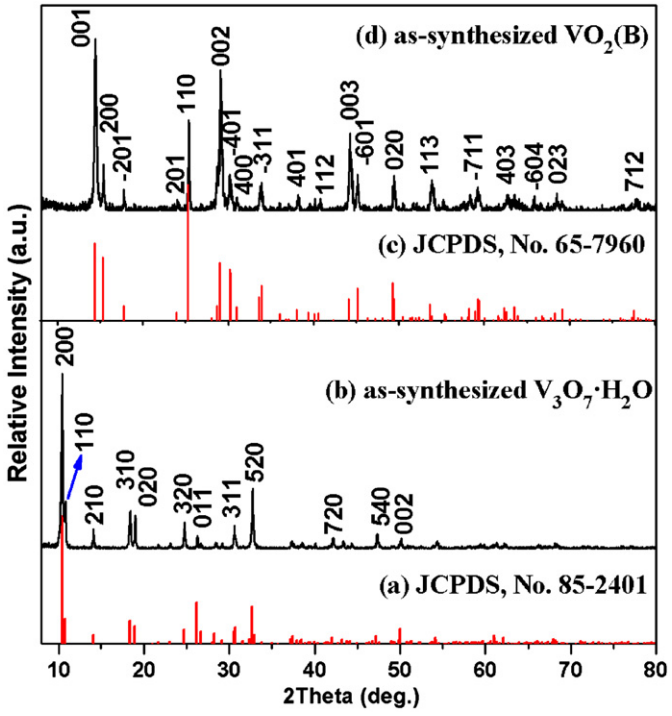

Fig. 1. XRD patterns of the as-obtained samples: (a) the standard JCPDS plots of $V_3O_7 \cdot H_2O$; (b) the as-synthesized $V_3O_7 \cdot H_2O$ nanobelts; (c) the standard JCPDS plots of VO_2(B); (b) the as-synthesized VO_2(B) nanobelts.

3. Results and discussion

3.1. The characterization of $V_3O_7 \cdot H_2O$ and VO_2(B) nanobelts

Fig. 1 shows the typical XRD patterns of the as-obtained $V_3O_7 \cdot H_2O$ and VO_2(B) nanobelts. All the diffraction peaks from Fig. 1b can be readily indexed to orthorhombic crystalline phase (space group: Pnam) of $V_3O_7 \cdot H_2O$ (JCPDS No. 85–2401, a = 16.929 Å, b = 9.359 Å, c = 3.644 Å) [37], whose plots are shown in Fig. 1a. No peaks of any other phases are detected from the XRD pattern, revealing the as-prepared product with high purity. In a similar method, it can be observed from Fig. 1d, that all the diffraction peaks can readily indexed as the monoclinic crystalline phase (space group C2/m) of VO_2(B) (JCPDS, No. 65-7960) [38] and the as-prepared VO_2(B) is high purity compared Fig. 1c and d.

The composition and vanadium valence state of the surface of the as-obtained $V_3O_7 \cdot H_2O$ and VO_2(B) nanobelts were further investigated by XPS, as shown in Fig. 2. The survey spectra reveal the as-prepared samples only consisting of vanadium and oxygen (The C_{1s} peak appears, which may be due to some CO_2 absorbed on the surface of the samples). It was reported [35,39–42] that $V^{5+}_{2p1/2}$ peak is located at about 524.3 eV and $V^{5+}_{2p3/2}$ peak is located at 516.9–517.7 eV; $V^{4+}_{2p1/2}$ peak is located at about 523.4 eV and $V^{4+}_{2p3/2}$ peak is located at 515.7–516.2 eV; and $V^{3+}_{2p1/2}$

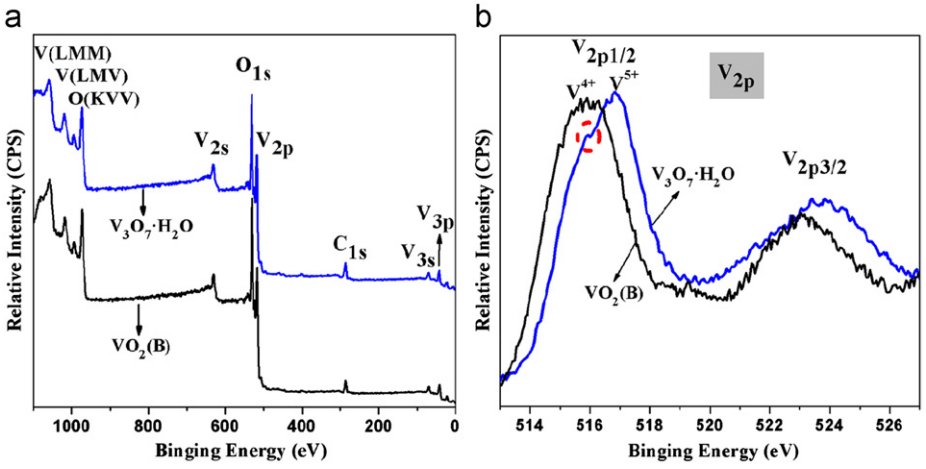

Fig. 2. XPS spectra of the as-obtained $V_3O_7 \cdot H_2O$ and VO_2(B) nanobelts: (a) the survey spectra; (b) the core-level spectra of V_{2p}.

peak is located at about 523.0 eV and $V^{3+}_{2p3/2}$ peak is located at 515.2–515.9 eV. As can be seen from Fig. 2b, the binding energies of $V_{2p1/2}$ and $V_{2p3/2}$ of $V_3O_7 \cdot H_2O$ centered at 524.3 and 516.9 eV are well consistent with the above results of V(V). However, we can also observe a weak intensity peak at around 516.9 eV, which represents the +4 oxidation state of vanadium. As for the as-obtained VO_2(B) nanobelts, the binding energies located at 515.9($V_{2p3/2}$) and 523.1 eV ($V_{2p1/2}$) are the characteristic of vanadium in the +4 oxidation state. Therefore, the core-level spectra of V_{2p} further confirm that the as-obtained $V_3O_7 \cdot H_2O$ nanobelts consist of V(V) and V(IV), while VO_2(B) nanobelts contain V(IV).

To get more information about the composition of the as-synthesized $V_3O_7 \cdot H_2O$ nanobelts, the corresponding FT-IR and TG measurements were carried out. The results are shown in *Supplementary data* (Figs. S1–S3), which further reveal that the as-obtained sample is $V_3O_7 \cdot H_2O$.

The morphology and size of the products were investigated by SEM and TEM. Fig. 3 shows the typical SEM and TEM images of the as-prepared $V_3O_7 \cdot H_2O$ nanobelts. The SEM image (Fig. 3a) indicates the as-obtained $V_3O_7 \cdot H_2O$ consists of a large number of 1 D nanobelts with length in the range of several to tens of micrometers and width ranging from 100 to 300 nm. A lower magnification TEM (Fig. 3b) image is consistent with the SEM image in width and length of nanobelts. It can be observed from the higher magnification TEM (Fig. 3c) image that the individual nanobelt has the smooth surface. The microstructure of the layered $V_3O_7 \cdot H_2O$ nanobelts was studied by SAED corresponding to the region as indicated by the square shown in Fig. 3d. The analysis of the SAED pattern reveals that the as-synthesized $V_3O_7 \cdot H_2O$ nanobelts grow along the [001] orientation, in agreement with Ref. [20]. Fig. 4 represents the typical SEM and TEM images of the as-prepared VO_2(B) nanobelts. It can be observed from Fig. 4a–c, that the as-obtained VO_2(B) consists of a large number of 1D nanobelts with length in the range of hundreds of nanometers to several micrometers and width ranging from 100 to 200 nm. Compared Fig. 3b and c with Fig. 4b and c, the crystallization of the as-obtained VO_2(B) nanobelts is worse than that of $V_3O_7 \cdot H_2O$ nanobelts, which can be further proved by the SAED pattern (Fig. 4d) of Fig. 4c.

3.2. Some parameters controlling the phase and morphology of the resulting products

As other low dimensional nanomaterials, some special conditions are required to synthesize the regular $V_3O_7 \cdot H_2O$ and VO_2(B) nanobelts. In this paper, we took the fabrication of $V_3O_7 \cdot H_2O$ nanobelts as the example to

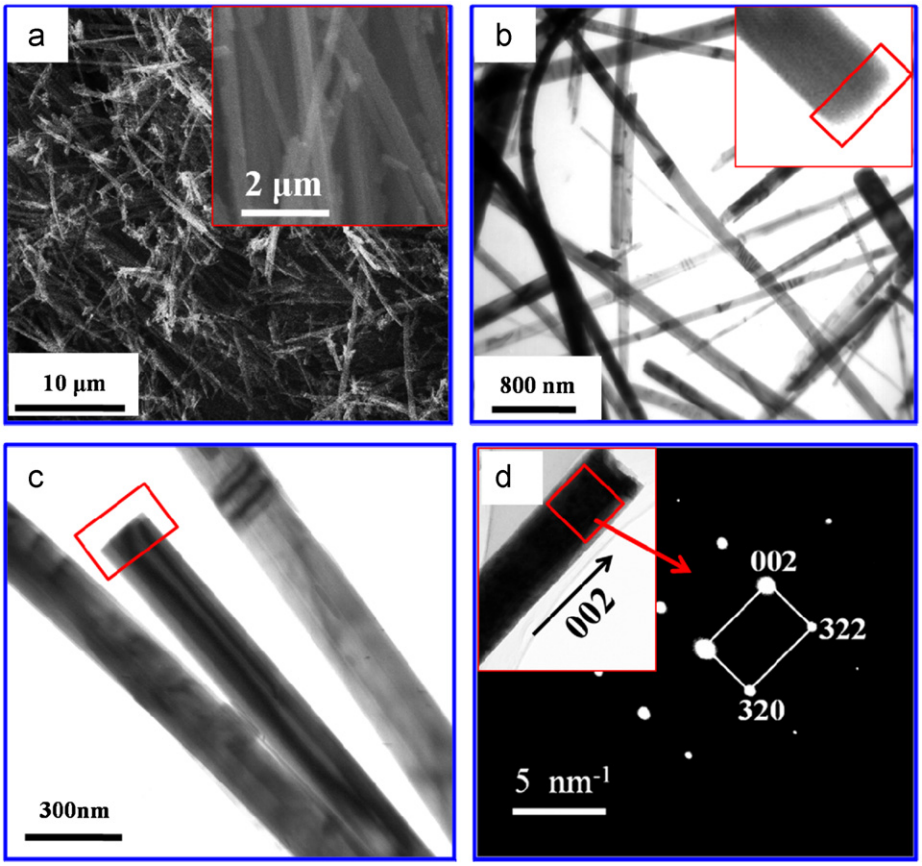

Fig. 3. Typical SEM and TEM images of the as-obtained $V_3O_7 \cdot H_2O$ nanobelts: (a) SEM, inset a higher magnification; (b) and (c) TEM; (d) the SAED pattern.

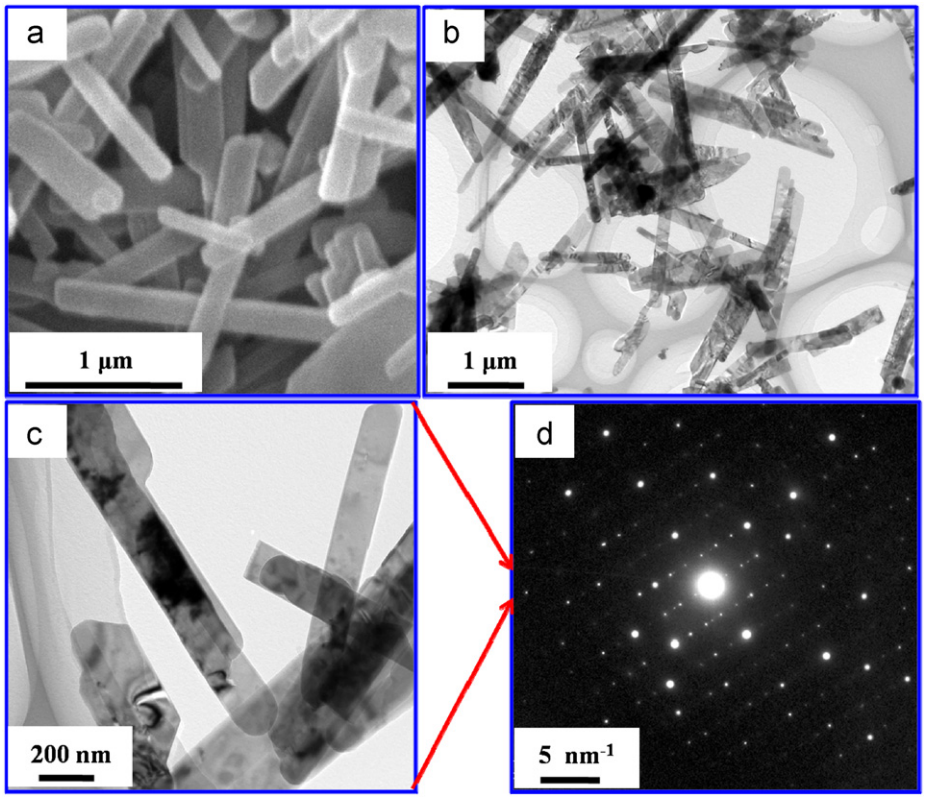

Fig. 4. Typical SEM and TEM images of the as-obtained VO_2(B) nanobelts: (a) SEM; (b) and (c) TEM; (d) the SAED pattern taken from (c).

reveal that some parameters (i.e.: the reaction temperature, the reaction time and the ratio of ethanol/water) have influenced on controlling the phase and morphology of the resulting products and the formation mechanism of vanadium oxides nanobelts.

3.2.1. *The reaction temperature*

It was found that the reaction temperature was a significant factor for preparing $V_3O_7 \cdot H_2O$ nanobelts. The detailed results and discussion are represented in *Supplementary data* (Fig. S4). The results indicate that the temperature (at 180 °C) is favorable for the fabrication of $V_3O_7 \cdot H_2O$ nanobelts.

3.2.2. *The ratio of ethanol/water*

The ratio of ethanol/water also played a major role in synthesizing the vanadium oxides nanobelts and it was found that $V_3O_7 \cdot H_2O$ and VO_2(B) nanobelts could be selectively synthesized by changing the quantity of ethanol. Keeping other parameters constant (23 mL of ethanol and deionized water), only the ratio of ethanol/water was considered as the changeable parameter. The synthetic reactions were carried out with different volume of ethanol (0, 0.05, 0.1, 0.2, 0.5, 1, 2, 5, 10 and 23 mL) at 180 °C for 12 h. The as-obtained samples were characterized by XRD and the corresponding results were summarized in Table 1. The results revealed that the redox reaction could not perform without ethanol. It was to say that ethanol acted as the reducing agent in the system. The phase of $V_3O_7 \cdot H_2O$ was obtained when a little of ethanol was used. With the volume of ethanol increased, the reductive capability in the system was strengthened, resulting that more and more vanadium atoms in the +5 oxidation state were reduced to that of +4 oxidation state. Finally, pure VO_2(B) was synthesized with 1.0 mL or more ethanol added. Figs. 3–5 show the TEM images of the samples synthesized with different volumes of ethanol: 0.05 (Fig. 5a), 0.1 (Fig. 3), 0.2 (Fig. 5b), 0.5 (Fig. 5c), 1 (Fig. 4), 2 (Fig. 5d), 5 (Fig. 5e) and 10 mL (Fig. 5f). When the volume of ethanol was 0.05–0.2 mL, large-scale of $V_3O_7 \cdot H_2O$ nanobelts were obtained (Fig. 5a, Fig. 3 and Fig. 5b). With 1 mL or more ethanol used, VO_2(B)

Table 1
Phases obtained by hydrothermal synthesis for different ethanol/water ratios. (Reaction conditions: 0.91 g of V_2O_5, 2 mL of H_2O_2, and at 180 °C for 12 h.).

Sample	EtOH/mL	H_2O/mL	Phase (XRD)
1	0	23	V_2O_5
2	0.05	22.95	$V_3O_7 \cdot H_2O$ and $VO_x \cdot nH_2O$
3	0.1	22.9	$V_3O_7 \cdot H_2O$
4	0.2	22.8	$V_3O_7 \cdot H_2O$
5	0.5	22.5	Main $V_3O_7 \cdot H_2O$ and minor VO_2(B)
6	1	22	VO_2(B)
7	2	21	VO_2(B)
8	5	18	VO_2(B)
9	10	13	VO_2(B)
10	23	0	VO_2(B)

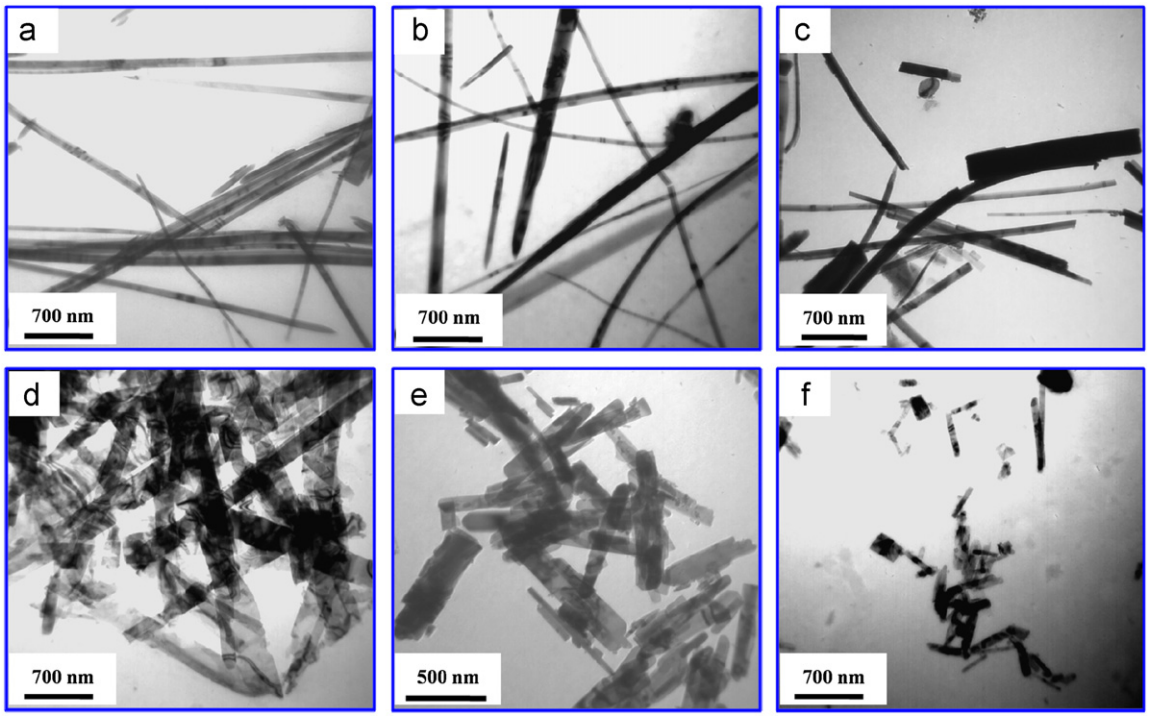

Fig. 5. TEM images of the as-prepared samples with different volumes of ethanol: (a) 0.05 mL; (b) 0.2 mL; (c) 0.5 mL; (d) 2 mL; (e) 5 mL; (f) 10 mL.

nanobelts were synthesized (Fig. 4 and Fig. 5d–f). However, it could be clearly observed from the TEM images that, the length of the as-obtained vanadium oxides nanobelts became shorter and shorter with the volume of ethanol increased (the more ethanol, the shorter nanobelts). Although the reason was not clear at our current knowledge, we presumed that it may be attributed to the function of ethanol or that the growth of VO_2(B) was slower than $V_3O_7 \cdot H_2O$ in one direction under the hydrothermal condition. Therefore, the ratio of ethanol/water was a critical factor for synthesizing vanadium oxides nanomaterials with different compositions and morphologies.

3.2.3. *The reaction time*

To reveal the evolution processes of the formation of $V_3O_7 \cdot H_2O$ nanobelts, the reaction time was changed with other parameters unchanged in our designed experiments. The synthetic process was ceased at definite reaction periods of 0.5, 2, 4, 6, 12, 24 and 48 h, and the as-obtained intermediate products were separated for XRD and TEM tests, which were respectively shown in Fig. S5 (*Supplementary data*) and Fig. 6. When the reaction was carried out for 0.5 h, the brown colloid solution was obtained and the XRD pattern (Fig. S5a) of its dried solid showed that it was main phase of V_2O_5 (JCPDS, No. 72-598). But we conjectured that this dried powder might contain some +4 oxidation state of vanadium. To verify this idea, the reaction using only this powder and redistilled water was carried out at 180 °C for 12 h, and the mixture of $V_3O_7 \cdot H_2O$ (main) and V_2O_5 were obtained, which was corresponding to the previous report [43]. With the reaction time increased to 2 or 4 h (Fig. S5b and c), the diffraction peaks of the intermediate products could be indexed as a set of peaks characteristic of the 00*l* reflections for the layered phase of $V_2O_5 \cdot xH_2O$, which was consistent with the reported data [44,45]. The as-obtained hydrate vanadium oxides were also treated with redistilled water at 180 °C for 12 h, respectively, and good crystal $V_3O_7 \cdot H_2O$ was obtained. When the reaction prolonged to 6 h, all the diffraction peaks could be indexed as the orthorhombic phase of $V_3O_7 \cdot H_2O$, indicating that the pure phase of orthorhombic $V_3O_7 \cdot H_2O$ was obtained (Fig. S5d). After heating 12, 24 and 48 h, the pure phase of orthorhombic $V_3O_7 \cdot H_2O$ with good crystalline structure was synthesized (Fig. S5e–g).

Fig. 6 displays the morphological evolution of the intermediate products during our synthetic route. After 0.5 h, a large number of vanadium oxides nanosheets and fragments were obtained (Fig. 6a), which indicated that the nanobelts were not formed. With the reaction time expanding to 2 h, the trend of nanobelts began to appear, as shown in Fig. 6b. As the reaction time increased, the amount of initial sheets and particles decreased. Some short nanobelts were formed after 4 h, although some scraps were still existed (Fig. 6c). With the reaction time extended to 6 h, a large number of vanadium oxides nanobelts had been explosively formed (Fig. 6d). The nanobelts had a length in the vast ranges of several to hundreds of micrometers and width ranging from about 40 to 140 nm, respectively, but we could occasionally see some fragments. The $V_3O_7 \cdot H_2O$ nanobelts were formed well after 12 h (Fig. 3 and Fig. 6e). When the reaction time reached to 24 h, the width of the as-obtained nanobelts

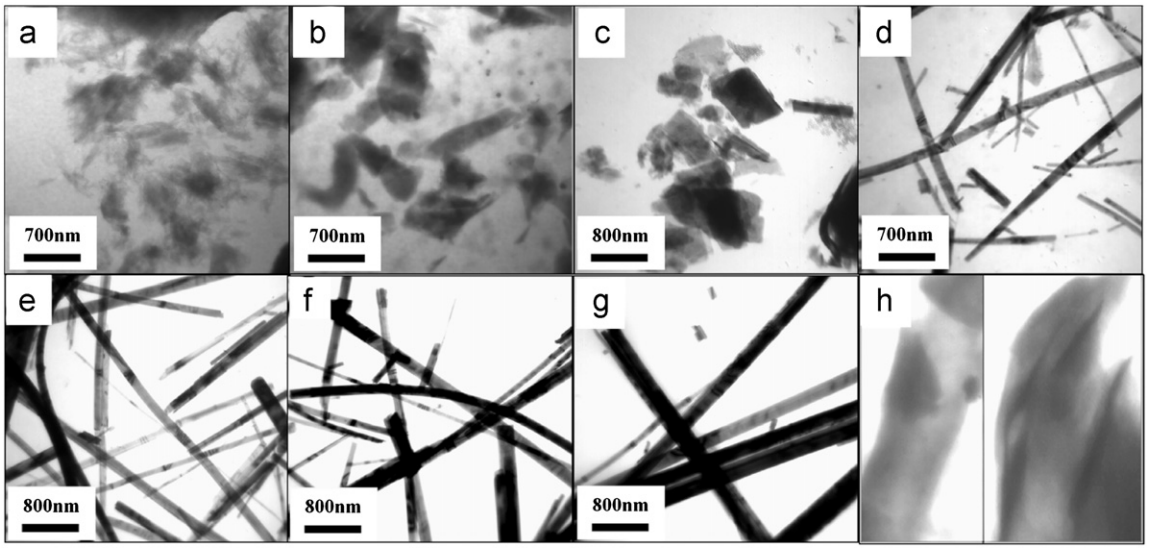

Fig. 6. TEM images of the as-prepared vanadium oxide nanobelts at different reaction time: (a) 0.5 h; (b) 2 h; (c) 4 h; (d) 6 h; (e) 12 h; (f) 24 h; (g) 48 h; (h) some evidences for folding taking from (b).

was increased to about 120–350 nm, as shown in Fig. 6f. After 48 h, the TEM image (Fig. 6g) revealed that the product mainly consisted of belts with a length of about tens to hundreds of micrometers and the width in the range 150–370 nm, which leads to the formation of belts with an ultrahigh-aspect-ratio. Based on the above analyses, with the increase in the reaction time, the belts began to form and became longer and the fragments became fewer, meanwhile the width and the thickness were also grown.

3.3. The formation mechanism

To study the formation mechanism of as-obtained vanadium oxides nanobelts, a series of experiments were explicitly performed. We proposed the reaction mechanism and the growth mechanism according to our researches. In the synthetic progress, the vanadium oxides nanobelts were successfully prepared via two steps: In the first step, the bulk V_2O_5 powders were completely dissolved in dilute H_2O_2 aqueous solution to get the deep orange solution and the $[VO(O_2)_2]^-$ was formed [25,46], as seen in Eq. (1). In the second step, some vanadium in the +5 oxidation state ($[VO(O_2)_2]^-$) was reduced to that of +4 oxidation state in the presence of ethanol, and the vanadium oxides crystal nuclei were appeared and constituted freely to form single-crystalline nanobelts under the hydrothermal conditions. In this progress, the ethanol played as the reducing agent and was oxidized to aldehyde [47–49], as shown in Eqs. (2) and (3). The effect of ethanol in this progress was verified by the following experiment: When only the water was used as the solvent, V_2O_5 was obtained. When ethanol was used, aldehyde as the oxidizing product was experimentally confirmed by the silver mirror reaction and gas chromatography (GC) analysis of the final solution mixture, which was collected, distilled and characterized. Thus, the reaction equations of $V_3O_7 \cdot H_2O$ and VO_2(B) through the reaction of V_2O_5, H_2O_2, EtOH and H_2O under the hydrothermal condition could be expressed as follows:

$$V_2O_5 + 4H_2O_2 \rightarrow 2[VO(O_2)_2]^- + 3H_2O + 2H^+; \quad (1)$$

$$6[VO(O_2)_2]^- + 6H^+ + CH_3CH_2OH \rightarrow 2V_3O_7 \cdot H_2O + CH_3CHO + 6O_2 + 2H_2O; \quad (2)$$

$$2[VO(O_2)_2]^- + 2H^+ + CH_3CH_2OH \rightarrow 2VO_2 + CH_3CHO + 2O_2 + 2H_2O. \quad (3)$$

To further study the growth mechanism of vanadium oxides nanobelts, we took the synthesis of $V_3O_7 \cdot H_2O$ nanobelts as the example to reveal its growth mechanism. To study the growth mechanism of $V_3O_7 \cdot H_2O$ nanobelts, three questions must be seriously considered, which are as follows: (1) The reducing reaction was firstly happened, then the growth of the $V_3O_7 \cdot H_2O$ nanobelts was evolved; (2) The vanadium oxide nanobelts were firstly grown well, then the reducing reaction happened; (3) The reducing reaction happened in conjunction with the growth progress. To solve this question, consideration experiments were carried out. First, the powder products obtained at the conditions [(a): 180 °C, 0.5 h; (b): 180 °C, 1 h; (c): 180 °C, 2 h;] with the other parameters unchanged were main phase V_2O_5 and (or) $V_2O_5 \cdot xH_2O$ confirmed by XRD. The final solution mixture was analyzed by GC after distillation and the results indicated the solution contained aldehyde after the reaction. These powder products after the above reactions were treated with only redistilled water at 180 °C for 12 h. After the reaction, the results were as follows: (a) the mixture of $V_3O_7 \cdot H_2O$ (main) and V_2O_5; (b) and (c) $V_3O_7 \cdot H_2O$. The above results were accordance with the previous reports [32,50]. Second, the reaction with 2 mL of ethanol at 180 °C for 0.5 h without changing other parameters was carried out, and the blue–green products were obtained, which was the

color of $V_3O_7 \cdot H_2O$. The dried products were treated using the above method (redistilled water, 180 °C, 12 h) and the good crystal $V_3O_7 \cdot H_2O$ was obtained. The collected solution after the reaction (2 mL of ethanol, 180 °C, 0.5 h) was characterized by the silver mirror reaction and GC, revealed the solution after the reaction contained ethanol and aldehyde. Therefore, we could conclude that the reducing reaction happened fast, then the growth of the $V_3O_7 \cdot H_2O$ nanobelts was evolved.

On the basis of the above results, time-dependent experiments were performed to gain an insight into the formation process of the samples characterized by TEM (Fig. 6) and the possible formation mechanism was proposed. We suggest that the formation of $V_3O_7 \cdot H_2O$ nanobelts is reasonably illuminated by a nucleation, crystallization, redissolve, recrystallization process, which can be expressed by a detailed model, as shown in Fig. 7. First, the $[VO(O_2)_2]^-$ in the system is formed by V_2O_5, H_2O and H_2O_2. At the beginning of the reaction, V(V) is partly reduced to V(IV) and the $V_3O_7 \cdot H_2O$ nuclei are formed and these nuclei rapidly develop into many pieces and fragments under the hydrothermal condition (Fig. 6a and b). Second, with the heating time extending, the pieces are aggregated, combined and folded (Fig. 6h), leading to the trend of nanobelts (Fig. 6c) and the vanadium oxide ribbon-like structures are a single burst of formation (Fig. 6d), while some nuclei and pieces are also formed and some fragments are still existed. In this course, interlayer force makes the pieces to aggregate and fold to form the short ribbon-like structures due to the layer structure of the vanadium oxides. Some evidences are found in the enlarged TEM images, as shown in Fig. 6h. Third, the short ribbon-like structures are grown into vanadium oxide nanobelts due to its crystal growth propensity because no templates or surfactants presents. Since nucleation, dissolution, and re-crystallization are typical steps in a hydrothermal synthesis process [51], some fragments and uncrystallized nanostructures are dissolved to improve the crystal nanobelts to grow sufficiently [52]. The reason is that the width and thickness become broad compared with the results by prolonging hydrothermal time, we can also say that the width and thickness is also grown in pace with the length, which indicates that the $V_3O_7 \cdot H_2O$ nanobelts grow along all directions. Because of crystal growth anisotropy and propensity, the $V_3O_7 \cdot H_2O$ nanobelts grow well as highly orient. From above discussions we can conclude that the formation of $V_3O_7 \cdot H_2O$ nanobelts is a nucleation, crystallization, redissolve, recrystallization process, in which the irregular uncrystallized structures are re-dissolved into the solution phase and the crystal nanobelts grow better. This formation mechanism is similar to the formation process of silver nanowires [53,54] and our previous report [20].

3.4. Electrochemical properties of $V_3O_7 \cdot H_2O$ and $VO_2(B)$ nanobelts

The vanadium oxides (i.e.: V_2O_5, V_3O_7, V_6O_{13}, VO_2, etc.) and their derivatives have attracted increasing attention because they can be used as the electrode materials for electrochemical applications in recent years. As the intercalation compounds, $V_3O_7 \cdot H_2O$ and VO_2(B) are promising cathode materials in lithium-ion batteries [20,23,24,26,55–57]. It was reported that the electrochemical properties of the electrode materials were influenced by many factors, such as intrinsic structure, morphology, and preparation methods. Therefore, in this paper, we also investigated the charge–discharge capability of $V_3O_7 \cdot H_2O$ and VO_2(B) nanobelts.

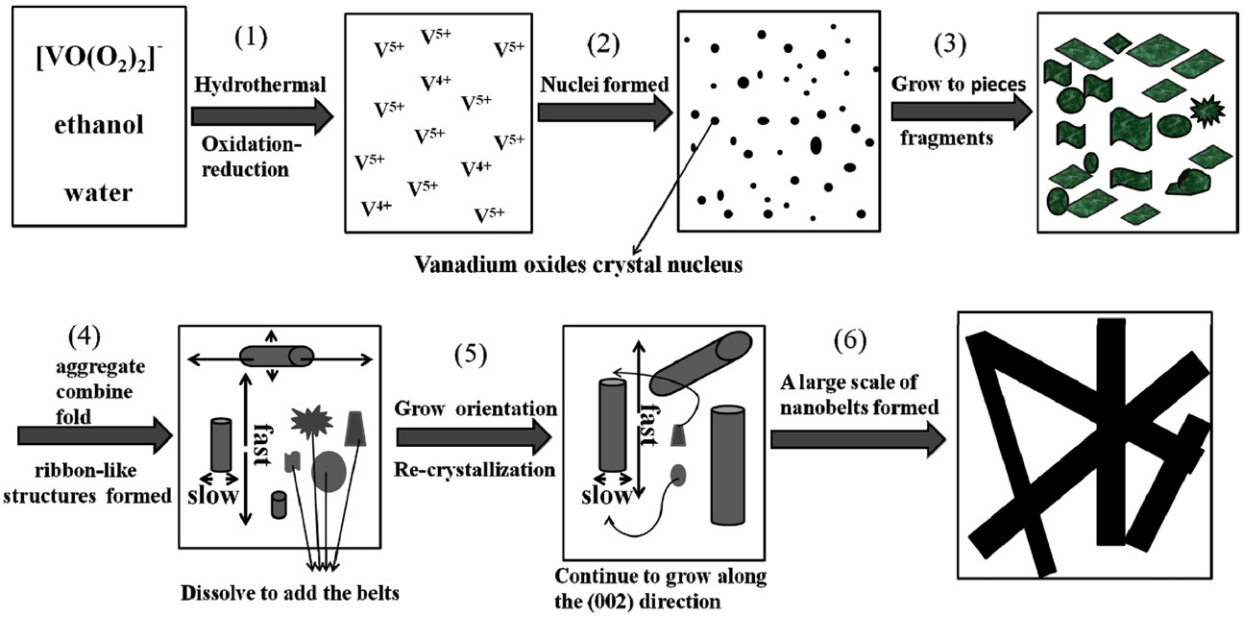

Fig. 7. Schematic illustration of the growth mechanism of the $V_3O_7 \cdot H_2O$ nanobelts.

The lithium-ion intercalation and deintercalation process could be described by the following equations:

$$V_3O_7\ H_2O + xLi + xe^- \rightleftharpoons Li^+ V_3O_7\ H_2O$$

$$VO_2 + Li + xe^- \rightleftharpoons Li^+ xVO_2$$

Fig. 8a shows the relationship between the cycle performance of specific capacity and the cycle number for the electrodes composed of the as-obtained $V_3O_7 \cdot H_2O$ or VO_2(B) nanobelts in a voltage range 4.0–1.5 V and under a constant current density of 30 mA/g. Obviously, $V_3O_7 \cdot H_2O$ nanobelts have better electrochemical properties than that of VO_2(B) nanobelts. As for $V_3O_7 \cdot H_2O$ nanobelts, we can see that the $V_3O_7 \cdot H_2O$ nanobelts exhibit an initial discharge capacity of as high as 350 mAh/g, which is much higher than the previous value [24]. The $V_3O_7 \cdot H_2O$ nanobelts with an initial high discharge capacity may be attributed to the large surface area and short diffusion distance resulting from the nanostructures [58,59]. The capacity of $V_3O_7 \cdot H_2O$ nanobelts moderately decays to 307 mAh/g in the second cycle, which retains about 87.7% of the initial discharge capacity. After that, the capacities are slightly decreased with the cycle number increased. It reaches a capacity of 223 mAh/g after 40 cycles, which retains about 63.7% of the initial discharge capacity. A small drop in the discharge capacity might be explained two following reasons: (1) Lithium ions are inserted into $V_3O_7 \cdot H_2O$ to form $Li_xV_3O_7 \cdot H_2O$. Correspondingly, lithium ions are reinserted from $Li_xV_3O_7 \cdot H_2O$ in this progress. However, some lithium ions cannot be completely extracted from the $Li_xV_3O_7 \cdot H_2O$ structure. This results in the small drop in the discharging capacity with the cycle number increased [24]; (2) The decrease of discharge capacity of the sample is likely due to partial fracture of its shape and structural degradation after the redox cycle. That has been studied during the charge–discharge process of vanadium oxides nanostructures [23,26,60]. In the case of VO_2(B) nanobelts, they exhibit an initial discharge capacity of 190 mAh/g. It delays to a capacity of 125 mAh/g after 40 cycles, which retains about 65.8% of the initial discharge capacity. Good rate capability is one of the keys in developing high power/fast charging lithium ion batteries. The cycling responses of the $V_3O_7 \cdot H_2O$ and VO_2(B) nanobelts electrodes at different current rates are investigated (4.0–1.5 V) and are shown in Fig. 8b. The first discharge capacities of $V_3O_7 \cdot H_2O$ nanobelts are 335, 253 and 204 mAh/g at current densities of 50, 100 and 200 mA/g, respectively. The capacity retention at every 10 cycles is 85.9% at 50 mA/g, 72.5% at 100 mA/g and 56.4% at 200 mA/g of the initial discharge capacity. As for VO_2(B) nanobelts, the first discharge capacities are 176, 131 and 101 mAh/g at current densities of 50, 100 and 200 mA/g, respectively. The capacity retention at every 10 cycles is 82.4% at 50 mA/g, 69.9% at 100 mA/g and 55.7% at 200 mA/g of the initial discharge capacity. All these results indicate that the $V_3O_7 \cdot H_2O$ and VO_2(B) nanobelts synthesized by this one-pot hydrothermal method are promising cathode materials in lithium ion batteries, and $V_3O_7 \cdot H_2O$ nanobelts have better electrochemical properties.

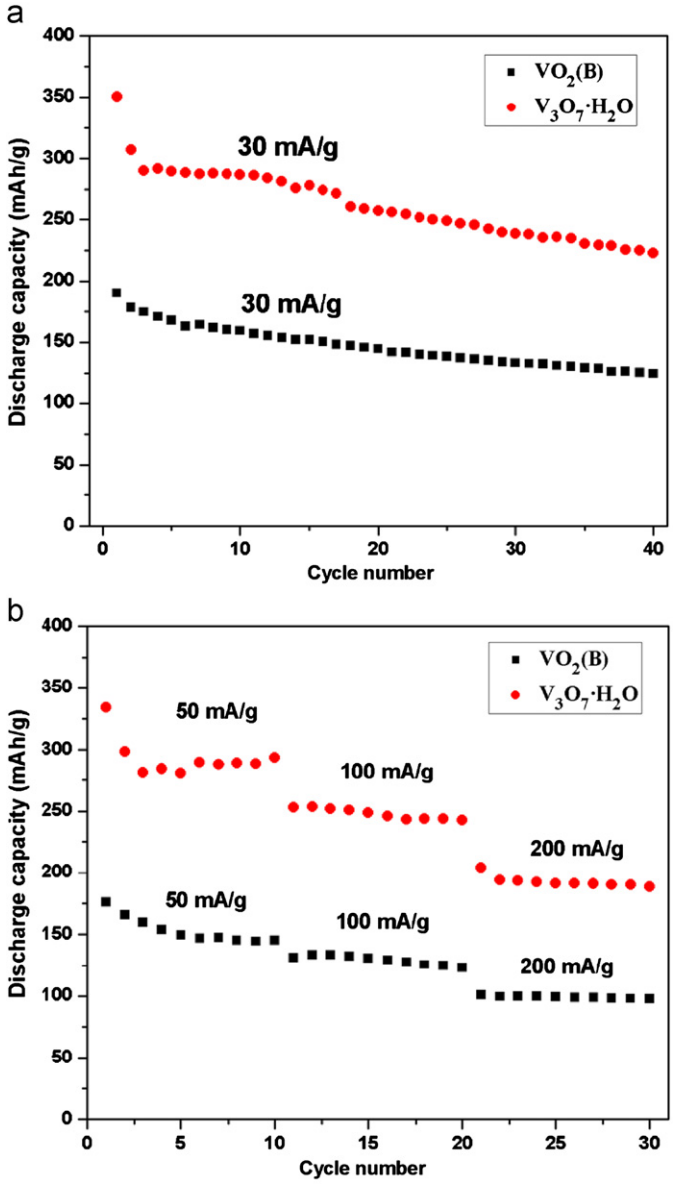

Fig. 8. (a) The cycle performances of the as-obtained $V_3O_7 \cdot H_2O$ and VO_2(B) nanobelts at a current density of 30 mA/g; (b) Discharge capacities of $V_3O_7 \cdot H_2O$ and VO_2(B) electrodes at various current densities of 50 to 200 mA/g.

3.5. The irreversible transformation of VO_2(B) to VO_2(M) nanobelts

In the past decades, many researchers have devoted their interest to synthesis and application of VO_2, because the metal–semiconductor transition temperature (T_c) of VO_2(M) is close to room temperature (68 °C) found by Morin [61]. Until now, VO_2(M) can be used in many areas [17], such as temperature sensing devices, optical switching devices, optical data storage media, intelligent thermochromic windows and so on. From the literature investigated, the methods of preparing

VO_2(M) are commonly treated other phase of VO_2 with high temperature at the inert atmosphere. Therefore, in this paper, we investigated the transformation from VO_2(B) nanobelts to VO_2(M) nanobelts by the thermal treatment, and it was found that VO_2(M) nanobelts could be converted from VO_2(B) nanobelts at 700 °C for 2 h under the inert atmosphere.

Fig. 9 represents the XRD patterns of the as-obtained VO_2(M) nanobelts. All the diffraction peaks from Fig. 9 can be readily indexed as monoclinic crystalline phase (space group: P21/c) of VO_2(M), which corresponds to the VO_2(M) (JCPDS, No. 72–0514, $a=5.743$, $b=4.517$, $c=5.375$ Å) already described in the literature [62]. No peaks of any other phases are detected from the XRD pattern, indicating the as-prepared VO_2(M) with high purity.

When the phase transition of VO_2(M) occurs, it respectively exhibits noticeable endothermal and exothermal profiles in the heating and cooling DSC curves, which corresponds to the phase transition $VO_2(M)=VO_2(R)$. Fig. 10 shows the representative DSC curves of VO_2(M) nanobelts with heating and cooling cycles. The T_c of VO_2(M) nanobelts is about 64 °C, which is a little lower than the reference [61]. It may be due to the size effect of the nanostructured materials. While the T_c is about 58 °C in the cooling cycle, which is due to the hysteresis behavior of VO_2(M) nanobelts. Besides, a TEM image (insert in Fig. 10) reveals that the morphology and size of the VO_2(M) are dependent on that of VO_2(B).

Based on the DSC curves of VO_2(M), it undergoes a noticeable endothermic peak at about 64 °C in the heating cycle and a noticeable exothermal at about 58 °C in the cooling cycle. It was reported that the drastic change occurred in its optical properties, accompanied by the phase transition of VO_2(M/R). Therefore, in this paper, the as-obtained VO_2(M) nanobelts was explored as an optical switching device. The optical switching properties of VO_2(M) was investigated by a series of variable-

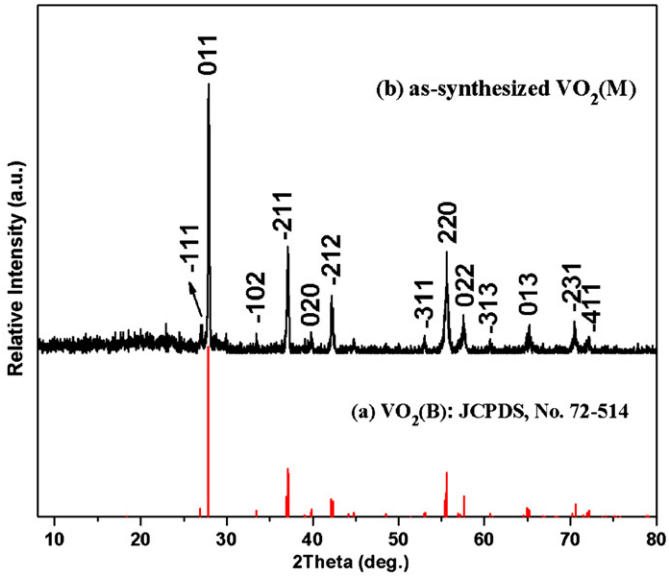

Fig. 9. XRD patterns of the as-obtained VO_2(M) nanobelts.

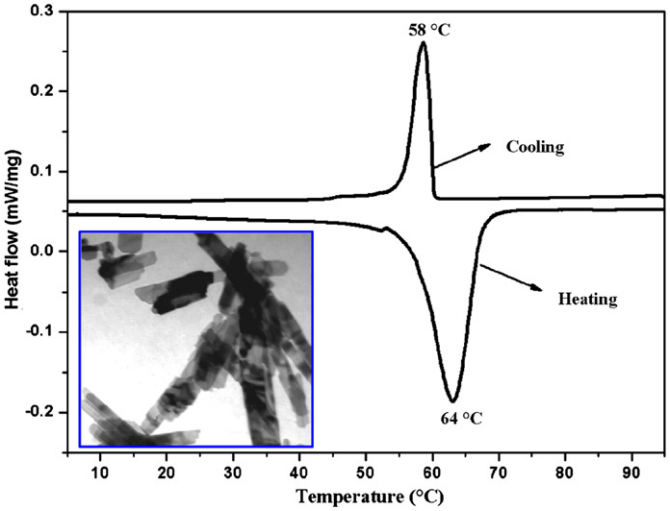

Fig. 10. DSC curves of the as-obtained VO_2(M) nanobelts with heating and cooling cycles, inserted a TEM image.

temperature IR of the heating and cooling cycles, as depicted in Fig. 11 and Fig. S6 (*Supplementary data*). Fig. 11a shows all the curves obtained with the variable-temperature IR tests. It can be clearly observed from Fig. 11a, that VO_2(M) nanobelts have the optical switching properties. To get a noticeable observation, two typical results below (15 °C) and above T_c (90 °C) are selected to make Fig. S6a, which reveal that the optical transmission of VO_2(M) nanobelts at 15 °C is higher than that at 90 °C, suggesting that VO_2(M) nanobelts converted from VO_2(B) nanobelts have good thermochromic properties. Furthermore, Fig. 11a and Fig. S6a both reveal that VO_2(M) nanobelts have potential applications in optical switching devices at the vibratory absorption bands from 1200 to 800 cm^{-1} due to its large transmission changes. Fig. S6b represents two IR curves below T_c from Fig. 11a: one is from the heating process, while the other is from the cooling process. These spectra have almost the same optical transmission, indicating that the phase transition of the as-obtained VO_2(M) nanobelts have good reversibility. Fig. 11b describes the process of the phase transition of VO_2(M) nanobelts before and after T_c, indicating its T_c is at about 66 °C in the heating cycle and at about 55 °C in the cooling cycle. However, the heating and cooling curves are asymmetric in Fig. 11a and b, which indicates the hysteresis behavior in the sample, in agreement with the DSC observation (Fig. 10). All of above properties of VO_2(M) nanobelts discussed from Fig. 11 and Fig. S6 verify that it is beneficial for the development and application of an optical switching material.

4. Conclusion

In conclusion, $V_3O_7 \cdot H_2O$ and VO_2(B) nanobelts were successfully synthesized by a template-free mild and direct hydrothermal reaction between peroxovanadium (V) complexes and green solvent (ethanol). Several parameters, such

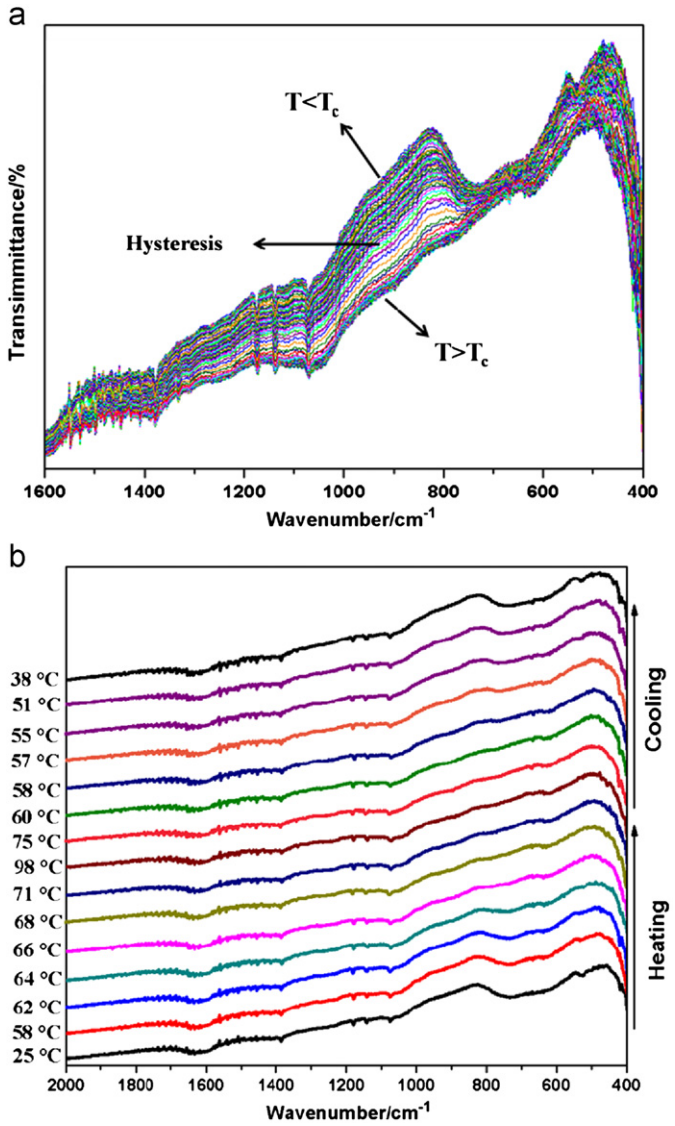

Fig. 11. Variable-temperature infrared spectra of the as-prepared VO_2(M) nanobelts: (a) All of IR curves with different temperatures; (b) Selected some typical IR curves from (a) to clearly reveal the process of the phase transition of VO_2(M) before and after T_c.

as the ratio of ethanol/water, the reaction temperature and the reaction time, were found to play an important role in controlling the morphologies and phases of the products. It was found that the ethanol was oxidized to aldehyde confirmed by the silver mirror reaction and gas chromatography. $V_3O_7 \cdot H_2O$ and VO_2(B) nanobelts could be selectively synthesized by controlling the quantity of ethanol. A nucleation, crystallization, redissolve, recrystallization process was proposed to explain the formation mechanism of vanadium oxides nanobelts. The electrochemical properties of $V_3O_7 \cdot H_2O$ and VO_2(B) nanobelts were studied, and they exhibited a high initial discharge capacity of 350 mAh/g and 190 mAh/g, respectively, indicating that these materials can be promising cathode materials in lithium-ion batteries. Furthermore, VO_2(M) nanobelts was prepared by the irreversible transformation of VO_2(B) nanobelts at 700 °C for 2 h under the inert atmosphere. The T_c of VO_2(M) nanobelts was about 64 °C. The optical switching properties of VO_2(M) nanobelts were investigated by variable-temperature IR, which revealed that the as-obtained VO_2(M) nanobelts could be applied to the optical switching devices.

Acknowledgment

This work was partially supported by the Fundamental Research Fund for the Central Universities, Independent Research Projects of Wuhan University (217274721), Luojia Young Scholars Program (217273483) and the Fourth Installment of Science and Technology Development 2010 Program of Suzhou (SYG201005).

Appendix A. Supplementary Information

Supplementary data associated with this article can be found in the online version at http://dx.doi.org/10.1016/j.ceramint.2012.06.001.

References

[1] G. Fasol, Nanowires: small is beautiful, Science (New York, NY) 280 (1998) 545–546.
[2] F. Caruso, Nanoengineering of particle surfaces, Advanced Materials (Weinheim, Germany) 13 (2001) 11–22.
[3] D. Sun, C.W. Kwon, G. Baure, E. Richman, J. Maclean, B. Dunn, S.H. Tolbert, The relationship between nanoscale structure and electrochemical properties of vanadium oxide nanorolls, Advanced Functional Materials 14 (2004) 1197–1204.
[4] X. Wang, J. Song, J. Liu, Z.L. Wang, Direct-current nanogenerator driven by ultrasonic waves, Science (New York, NY) 316 (2007) 102–105.
[5] Y. Qin, X.D. Wang, Z.L. Wang, Microfibre-nanowire hybrid structure for energy scavenging, Nature 451 (2008) 809–813.
[6] Z.W. Pan, Z.R. Dai, Z.L. Wang, Nanobelts of semiconducting oxides, Science (New York, NY) 291 (2001) 1947–1949.
[7] Y. Zhang, M. Fan, X. Liu, C. Huang, H. Li, Beltlike V_2O_3@C Core–Shell-structured composite: design, preparation, characterization, phase transition, and improvement of electrochemical properties of V_2O_3, European Journal of Inorganic Chemistry 2012 (2012) 1650–1659.
[8] Y. Zhang, M. Fan, F. Niu, W. Wu, C. Huang, X. Liu, H. Li, X. Liu, Belt-like VO_2(M) with a rectangular cross section: A new route to prepare, the phase transition and the optical switching properties, Current Applied Physics 12 (2012) 875–879.
[9] Y. Zhang, M. Fan, X. Liu, G. Xie, H. Li, C. Huang, Synthesis of VO_2(A) nanobelts by the transformation of VO_2(B) under the hydrothermal treatment and its optical switching properties, Solid State Communications 152 (2012) 253–256.
[10] Y. Zhang, M. Fan, F. Niu, Y. Zhong, C. Huang, X. Liu, B. Wang, H. Li, Hydrothermal synthesis of VO_2(A) nanobelts and their phase transition and optical switching properties, Micro and Nano Letters 6 (2011) 888–891.
[11] Y.F. Zhang, X.H. Liu, J.R. Nie, L. Yu, Y.L. Zhong, C. Huang, Improve the catalytic activity of α-Fe_2O_3 particles in decomposition of ammonium perchlorate by coating amorphous carbon on their surface, Journal of Solid State Chemistry 184 (2011) 387–390.
[12] J. Liu, X. Wang, Q. Peng, Y. Li, Vanadium pentoxide nanobelts: highly selective and stable ethanol sensor materials, Advanced Materials (Weinheim, Germany) 17 (2005) 764–767.

[13] D. Wang, L. Cao, J. Huang, J. Wu, Synthesis and electrochemical properties of LiV_3O_8 via an improved sol–gel process, Ceramics International 38 (2012) 2647–2652.
[14] S. Milošević, I. Stojković, S. Kurko, J.G. Novaković, N. Cvjetićanin, The simple one-step solvothermal synthesis of nanostructurated VO_2(B), Ceramics International 38 (2012) 2313–2317.
[15] J.-H. Cho, Y.-J. Byun, J.-H. Kim, Y.-J. Lee, Y.-H. Jeong, M.-P. Chun, J.-H. Paik, T.H. Sung, Thermochromic characteristics of WO_3-doped vanadium dioxide thin films prepared by sol–gel method, Ceramics International 38 (Supplement 1) (2012) S589–S593.
[16] Y.F. Zhang, X.H. Liu, D.Z. Chen, L. Yu, J.R. Nie, S.P. Yi, H.B. Li, C. Huang, Fabrication of $V_3O_7 \cdot H_2O$@C core-shell nanostructured composites and the effect of $V_3O_7 \cdot H_2O$ and $V_3O_7 \cdot H_2O$@C on decomposition of ammonium perchlorate, Journal of Alloys and Compounds 509 (2011) L69–L73.
[17] I.P. Parkin, T.D. Manning, Intelligent thermochromic windows, Journal of Chemical Education 83 (2006) 393–400.
[18] Y. Zhang, F. Zhang, L. Yu, M. Fan, Y. Zhong, X. Liu, Y. Mao, C. Huang, Synthesis and characterization of belt-like VO_2(B)@carbon and V_2O_3@carbon core–shell structured composites, Colloids Surface A 396 (2012) 144–152.
[19] Y. Zhang, M. Fan, W. Wu, L. Hu, J. Zhang, Y. Mao, C. Huang, X. Liu, A novel route to fabricate belt-like VO_2(M)@C core–shell structured composite and its phase transition properties, Materials Letters 71 (2012) 127–130.
[20] Y. Zhang, X. Liu, G. Xie, L. Yu, S. Yi, M. Hu, C. Huang, Hydrothermal synthesis, characterization, formation mechanism and electrochemical property of $V_3O_7 \cdot H_2O$ single-crystal nanobelts, Materials Science and Engineering B 175 (2010) 164–171.
[21] Y. Zhang, Y. Huang, J. Zhang, W. Wu, F. Niu, Y. Zhong, X. Liu, X. Liu, C. Huang, Facile synthesis, phase transition, optical switching and oxidation resistance properties of belt-like VO_2(A) and VO_2(M) with a rectangular cross section, Materials research bulletin 47 (2012) 1978–1986.
[22] Y.F. Zhang, M. Zhou, M.J. Fan, C. Huang, C.X. Chen, Y.L. Cao, H.B. Li, X.H. Liu, Improvement of the electrochemical properties of $V_3O_7 \cdot H_2O$ nanobelts for Li battery application through synthesis of V_3O_7@C core-shell nanostructured composites, Current Applied Physics 11 (2011) 1159–1163.
[23] S. Gao, Z. Chen, K. MingdengWei, H. Wei, Zhou, Single crystal nanobelts of $V_3O_7 \cdot H_2O$: A lithium intercalation host with a large capacity, Electrochimica Acta 54 (2009) 1115–1118.
[24] H. Qiao, X. Zhu, Z. Zheng, L. Liu, L. Zhang, Synthesis of $V_3O_7 \cdot H_2O$ nanobelts as cathode materials for lithium-ion batteries, Electrochemistry Communications 8 (2006) 21–26.
[25] L. Yu, X. Zhang, Hydrothermal synthesis and characterization of vanadium oxide/titanate composite nanorods, Materials Chemistry and Physics 87 (2004) 168–172.
[26] S. Shi, M. Cao, X. He, H. Xie, Surfactant-assisted hydrothermal growth of single-crystalline ultrahigh-aspect-ratio vanadium oxide nanobelts, Crystal Growth and Design 7 (2007) 1893–1897.
[27] G. Li, S. Pang, Z. Wang, H. Peng, Z. Zhang, Synthesis of $H_2V_3O_8$ single-crystal nanobelts, European Journal of Inorganic Chemistry 2005 (2005) 2060–2063.
[28] G.S. Zakharova, V.L. Volkov, C. Täschner, I. Hellmann, A. Leonhardt, R. Klingeler, B. Büchner, Synthesis and characterization of $V_3O_7 \cdot H_2O$ nanobelts, Solid State Communications 149 (2009) 814–817.
[29] X. Liu, C. Huang, S. Yi, G. Xie, H. Li, Y. Luo, A new solvothermal method of preparing VO_2 nanosheets and petaloid clusters, Solid State Communications 144 (2007) 259–263.
[30] J.A. Ni, W.T. Jiang, K. Yu, Y.F. Gao, Z.Q. Zhu, Hydrothermal synthesis of VO_2(B) nanostructures and application in aqueous Li-ion battery, Electrochimica Acta 56 (2011) 2122–2126.
[31] K. Yu, H.H. Yin, Z.L. Zhang, Z.Q. Zhu, Morphology-control of VO_2(B) nanostructures in hydrothermal synthesis and their field emission properties, Applied Surface Science 257 (2011) 8840–8845.
[32] Y. Wang, G.Z. Cao, Synthesis and enhanced intercalation properties of nanostructured vanadium oxides, Chemistry of Materials: a Publication of the American Chemical Society 18 (2006) 2787–2804.
[33] S.A. Corr, M. Grossman, Y.F. Shi, K.R. Heier, G.D. Stucky, R. Seshadri, VO_2(B) nanorods: solvothermal preparation, electrical properties, and conversion to rutile VO_2 and V_2O_3, Journal of Materials Chemistry 19 (2009) 4362–4367.
[34] S.D. Zhang, Y.M. Li, C.Z. Wu, F. Zheng, Y. Xie, Novel flowerlike metastable vanadium dioxide (B) micronanostructures: facile synthesis and application in aqueous lithium ion batteries, Journal of Physical Chemistry C 113 (2009) 15058–15067.
[35] X. Liu, G. Xie, C. Huang, Q. Xu, Y. Zhang, Y. Luo, A facile method for preparing VO_2 nanobelts, Materials Letters 62 (2008) 1878–1880.
[36] F. Sediri, N. Gharbi, Nanorod B phase VO_2 obtained by using benzylamine as a reducing agent, Materials Science and Engineering B 139 (2007) 114–117.
[37] Y. Oka, T. Yao, N. Yamamoto, Structure determination of $H_2V_3O_8$ by powder X-ray diffraction, Journal of Solid State Chemistry 89 (1990) 372–377.
[38] F. Theobald, R. Cabala, J. Bernard, Essai sur la structure de VO_2(B), Journal of Solid State Chemistry 17 (1976) 431–438.
[39] J. Mendialdua, R. Casanova, Y. Barbaux, XPS studies of V_2O_5, V_6O_{13}, VO_2 and V_2O_3, Journal of Electron Spectroscopy and Related Phenomena 71 (1995) 249–261.
[40] N. Alov, D. Kutsko, I. Spirovova, Z. Bastl, XPS study of vanadium surface oxidation by oxygen ion bombardment, Surface Science 600 (2006) 1628–1631.
[41] Y. Chen, K. Xie, Z.X. Liu, Determination of the position of V^{4+} as minor component in XPS spectra by difference spectra, Applied Surface Science 133 (1998) 221–224.
[42] G. Silversmit, D. Depla, H. Poelman, G.B. Marin, R.D. Gryse, Determination of the V2p XPS binding energies for different vanadium oxidation states (V^{5+} to V^{0+}), Journal of Electron Spectroscopy 135 (2004) 167–175.
[43] J. Livage, Synthesis of polyoxovanadates via chimie douce, Coordination Chemistry Reviews 180 (1998) 999–1018.
[44] F. Zhou, X. Zhao, C. Yuan, L. Li, Vanadium pentoxide nanowires: hydrothermal synthesis, formation mechanism, and phase control parameters, Crystal Growth and Design 8 (2008) 723–727.
[45] Y. Wang, H. Shang, T. Chou, G. Cao, Effects of thermal annealing on the Li^+ intercalation properties of $V_2O_5 \cdot nH_2O$ xerogel films, The Journal of Physical Chemistry B 109 (2005) 11361–11366.
[46] T.-D. Nguyen, T.-O. Do, Solvo-Hydrothermal, Approach for the shape-selective synthesis of vanadium oxide nanocrystals and their characterization, Langmuir: the ACS Journal of Surfaces and Colloids 25 (2009) 5322–5332.
[47] J. Ma, Q. Wu, Y. Chen, An oxides-hydrothermal approach from bulky V_2O_5 powder to $V_3O_7 \cdot H_2O$ nanoribbons or V_3O_7 nanoflowers in various ethanol/water mixed solvent, Materials Research Bulletin 44 (2009) 1142–1147.
[48] A. Butler, M.J. Clague, G.E. Meister, Vanadium Peroxide Complexes, Chemical Reviews 94 (1994) 625–638.
[49] O. Bortolini, V. Conte, Vanadium (V) peroxocomplexes: Structure, chemistry and biological implications, Journal of Inorganic Biochemistry 99 (2005) 1549–1557.
[50] W. Avansi, C. Ribeiro, E.R. Leite, V.R. Mastelaro, Vanadium pentoxide nanostructures: an effective control of morphology and crystal structure in hydrothermal conditions, Crystal Growth and Design 9 (2009) 3626–3631.
[51] R.I. Walton, Subcritical solvothermal synthesis of condensed inorganic materials, Chemical Society Reviews 31 (2002) 230–238.
[52] K. Chang, C. Hu, $H_2V_3O_8$ single-crystal nanobelts: Hydrothermal preparation and formation mechanism, Acta Materialia 55 (2007) 6192–6197.
[53] Y. Sun, Y. Xia, Large-scale synthesis of uniform silver nanowires through a soft, self-seeding, polyol process, Advanced Materials (Weinheim, Germany) 14 (2002) 833–837.

[54] Y. Sun, B. Gates, B. Mayers, Y. Xia, Crystalline silver nanowires by soft solution processing, Nano Letters 2 (2002) 165–168.
[55] M.M. Rahman, J.Z. Wang, N.H. Idris, Z.X. Chen, H.K. Liu, Enhanced lithium storage in a VO_2-multiwall carbon nanotube microsheet composite prepared via an in situ hydrothermal process, Electrochimica Acta 56 (2010) 693–699.
[56] H.M. Liu, Y.G. Wang, K.X. Wang, E. Hosono, H.S. Zhou, Design and synthesis of a novel nanothorn VO_2 hollow microsphere and their application in lithium-ion batteries, Journal of Materials Chemistry 19 (2009) 2835–2840.
[57] C.V.S. Reddy, E.H. Walker, S.A. Wicker, Q.L. Williams, R.R. Kalluru, Synthesis of VO_2 nanorods for Li battery application, Current Applied Physics 9 (2009) 1195–1198.
[58] S.H. Ng, S.Y. Chew, J. Wang, D. Wexler, Y. Tournayre, K. Konstantinov, H.K. Liu, Synthesis and electrochemical properties of V_2O_5 nanostructures prepared via a precipitation process for lithium-ion battery cathodes, Journal of Power Sources 174 (2007) 1032–1035.
[59] Y. Wang, K. Takahashi, H. Shang, G. Cao, Synthesis and electrochemical properties of vanadium pentoxide nanotube arrays, The Journal of Physical Chemistry B 109 (2005) 3085–3088.
[60] G.R. Patzke, F. Krumeich, R. Nesper, Oxidic nanotubes and nanorods—Anisotropic modules for a future nanotechnology, Angewandte Chemie-International Edition 41 (2002) 2446–2461.
[61] F.J. Morin, Oxides which show a metal-to-insulator transition at the neel temperature, Physical Review Letters 3 (1959) 34–36.
[62] G. Andersson, Studies on vanadium oxides. II. The Crystal structure of vanadium dioxide, Acta Chemica Scandinavica (Copenhagen, Denmark: 1989) 10 (1956) 623–628.